

# High-stability transfer of an optical frequency over long fiber-optic links

P. A. Williams,\* W. C. Swann, and N. R. Newbury

National Institute of Standards and Technology, 325 Broadway, Boulder, Colorado 80305, USA

\*Corresponding author: pwilliam@boulder.nist.gov

Received February 25, 2008; revised May 2, 2008; accepted May 31, 2008;  
posted June 9, 2008 (Doc. ID 93074); published July 17, 2008

We present theoretical predictions and experimental measurements for the achievable phase noise, timing jitter, and frequency stability in the coherent transport of an optical frequency over a fiber-optic link. Both technical and fundamental limitations to the coherent transfer are discussed. Measurements of the coherent transfer of an optical carrier over links ranging from 38 to 251 km demonstrate good agreement with theory. With appropriate experimental design and bidirectional transfer on a single optical fiber, the frequency instability at short times can reach the fundamental limit imposed by delay-unsuppressed phase noise from the fiber link, yielding a frequency instability that scales as link length to the 3/2 power. For two-way transfer on separate outgoing and return fibers, the instability is severely limited by differential fiber noise.

OCIS codes: 060.2360, 120.3930.

## 1. INTRODUCTION

Distribution of highly coherent, stable frequencies over a wide area is an important enabling tool in a variety of applications including the comparison of optical clocks, searches for variations in the fundamental constants, radio astronomy, particle physics, and broad baseline interferometry, as discussed in several recent review articles [1,2]. A challenge in the distribution of coherent frequency sources is how to transmit the coherent signal over long distances with minimal perturbation. Any variation in the path length connecting end sites results in a Doppler shift of the transmitted frequency, thereby degrading its phase noise and stability. A variety of techniques have been demonstrated to transport frequencies faithfully despite these Doppler shifts. A common-view global positioning satellite system (GPS) has traditionally been used, which allows flexibility in the receiver's position and fractional frequency stabilities of a few parts in  $10^{15}$  with one-day averaging [3]. Fiber-optic-based transmission provides an alternate method [1,2]. In one approach, a coherent, stabilized RF tone is transmitted over an optical fiber by use of the RF to modulate an optical carrier. In an alternative approach, a coherent, stabilized optical frequency is transmitted directly over fiber. The optical frequency can be converted to any other optical frequency or RF at the far end through an optical femtosecond frequency comb [4]. This approach yields the highest fractional frequency stabilities and is the one discussed here. Following initial demonstrations in the early 1990s on the transport of optical frequencies [5,6], several groups have recently explored transmission of an optical carrier over optical fiber at ever-increasing distances up to 251 km [4,7–10].

In this paper, we detail our theoretical and experimental efforts to determine the performance limitations for optical frequency transport through long optical fiber links building on our recently reported results [7]. We find two regimes of phase noise, or alternatively, frequency in-

stability. At low frequencies, interferometer noise (excess phase noise from the measurement system) dominates. For higher frequencies the noise suppression is limited by what we call delay-unsuppressed residual phase noise due to the transit time of the light in the fiber link (the delay). As is well known, delay in a feedback loop will limit the bandwidth and therefore the corresponding noise suppression. While this effect is present in our setup, here we are concerned with an entirely different consequence of the delay, which was pointed out in [7]. Because of the delay, the signal light exits the link at the far end before any correction can be sensed and applied at the transmit end. As a result, it is impossible to fully suppress the fiber link noise, and even if the round-trip noise is fully suppressed, the one-way signal light will still suffer from some unsuppressed fiber noise, this delay-unsuppressed noise is described in detail in Subsection 3.A and Appendix A. The graphs of Fig. 1 illustrate these two regimes for both phase noise and frequency instability. In general, the phase noise on the transmitted (remote) signal for the phase-locked system can be expressed as

$$S_{\text{remote}}(f) = S_{\text{Int}}(f) + S_D(f) + \text{other terms}, \quad (1.1)$$

where  $S_{\text{Int}}$  and  $S_D$  are the interferometric and delay-unsuppressed noise, respectively, and dominate other noise contributions for frequencies  $f$  below  $1/(4\tau)$  where  $\tau$  is the one-way propagation time along the link. Due to the low-frequency range of the interferometer-noise regime, we did not directly measure  $S_{\text{Int}}$  but inferred it from the frequency instability. The frequency instability on the remote signal is expressed as the modified Allan variance  $\sigma_{\nu, \text{remote}}^2$ . For the observed scaling of  $S_{\text{Int}} \propto f^{-2}$  and  $S_D \propto f^0$ , we derive

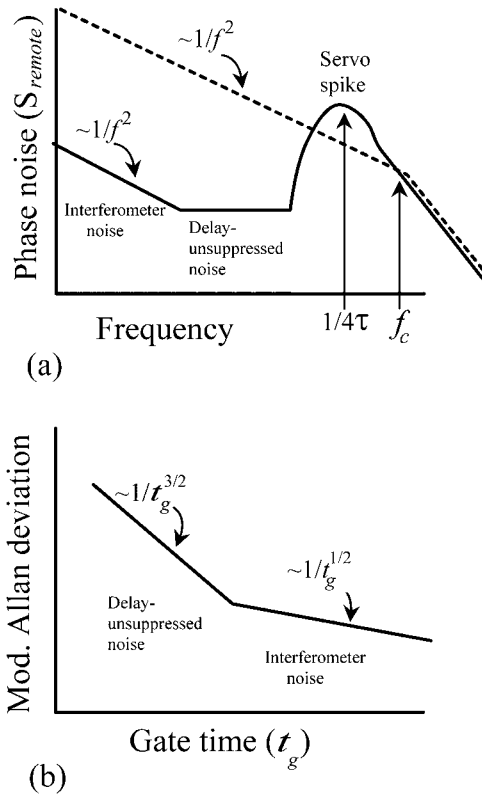


Fig. 1. Schematic of (a) phase noise and (b) frequency instability behavior for optimized optical frequency transfer over optical fiber. Dashed line indicates unlocked fiber phase noise; solid curves indicate phase noise and modified Allan deviation when the system is phase-locked.

$$\sigma_{v,\text{remote}}^2 = \kappa_{\text{Int}}^2/t_g + \kappa_D^2 L^3/t_g^3 + \text{other terms}, \quad (1.2)$$

where  $t_g$  is the gate time (averaging time of the frequency counter) in seconds and  $L$  is the link length in kilometers. The empirical constant  $\kappa_D$  characterizes the instability due to delay-unsuppressed fiber noise and is equal to  $\sim 8 \times 10^{-20} (\text{s/km})^{3/2}$  for our fiber link. The constant  $\kappa_{\text{Int}}$  characterizes the instability noise floor from the transmitter and receiver interferometers and is equal to  $\sim 2 \times 10^{-17} \text{ s}^{1/2}$  for our setup.

Section 2 outlines the basic experimental setup, which follows the well-established Doppler cancellation technique [5,6]. Section 3 discusses possible limitations due to both the link and the measurement systems. In Section 4, we present experimental results supporting Eqs. (1.1) and (1.2). The measurements of Section 4 used bidirectional optical fiber, i.e., the outgoing and return signals are carried on the same fiber strand. Most deployed fiber networks include optical isolators and do not support bidirectional transport. Section 5 discusses measurements where the outgoing and return signals propagate down different fiber strands within a single fiber bundle. We find this bidirectional transport is not competitive with satellite-based techniques.

## 2. EXPERIMENTAL SETUP

Thermal and acoustic fluctuations of the fiber link will Doppler-shift the transmitted frequency. The link can be

stabilized against these optical-path-length fluctuations by either physically modulating the path length or by intentionally shifting the frequency of light to cancel the Doppler shifts [1,2]. Physically modulating the path length through, for example, a piezoelectric fiber stretcher is impractical for long-distance transport because of its low dynamic range [1]. Furthermore, the birefringence associated with the fiber stretcher can couple with the fiber link polarization-mode dispersion (PMD) to degrade the frequency stability [11,12]. These drawbacks are avoided by instead compensating for the Doppler shift with an acousto-optic modulator (AOM) [5,6].

In an actual frequency transfer link, the remote end would be far from the local (source) end. However, testing the stable transport of an optical frequency requires that the fiber link forms a loop. In such a configuration, light exiting the link's remote end is located near the source for comparison. Figure 2 illustrates our setup where the local portion and remote portion of the setup are indicated. The stable optical frequency source is a 1535 nm cw fiber laser stabilized [13] to a stable optical cavity (finesse is 165,000; linewidth is 9 kHz) giving a linewidth of  $\sim 1$  Hz (coherence length  $\sim 3 \times 10^8$  m) over a 1.5 s observation time and a drift rate of a few Hz/s. An  $\sim 10$  m fiber link connects this laser to the setup. The added phase noise from this short fiber link is insignificant compared to the larger delay-unsuppressed link noise (see Subsection 3.C). Part of this source light is launched into the link, and part is split off to serve as a local oscillator (LO). Source light launched into the link passes through AOM1 (adding a nominal 80.5 MHz frequency shift) and propagates to the remote end, where it encounters AOM2, which provides an additional fixed 24 MHz frequency shift to distinguish light reflected at the remote end from stray reflections along the link [9,14]. Fifty percent of the light is retroreflected from the remote end, emerges from the start of the fiber, and is heterodyned against the LO light to yield a 209 MHz RF signal (twice the nominal 80.5 MHz shift of AOM1 plus twice the 24 MHz shift of AOM2). Assuming equal noise in the forward and return paths, this RF signal includes twice the phase noise of the one-way transmitted optical frequency. This 209 MHz signal is phase-locked to a RF synthesizer through feedback to AOM1 [5,6]. The response of this phase-locked loop (PLL) is analyzed in much more detail in Appendix A. It includes a  $16\times$  frequency divider on the heterodyned signal to provide the dynamic range necessary to maintain phase-lock despite large acoustic disturbances [14]. Heterodyne detection of the return light, in combination with the use of optical amplification in the 251 km link (discussed later), ensures close to shot-noise-limited signal-to-noise ratio (SNR) provided the polarizations states of the LO and return light are aligned using a fiber-optic polarization controller. Slow changes in the fiber-link birefringence (due to temperature or stress variation) will cause a drift in the polarization of the round-trip signal. To combat this, a partially reflecting (50%) Faraday mirror was used to reflect the round-trip signal so that it emerged from the fiber link with a polarization orthogonal to the input polarization state regardless of the fiber birefringence [15].

Although the PLL acts to cancel the phase noise on the

round-trip signal, its real purpose is to cancel the phase noise on the remote one-way signal. To test the noise reduction, the remote one-way signal was heterodyned against a portion of the source laser (LO) light at the remote detector, yielding a 104.5 MHz beat note that was analyzed for frequency stability and phase noise. Since this one-way signal does not benefit from the Faraday mirror, periodic adjustments of the polarization controllers in this branch were necessary.

Figure 2 shows erbium-doped fiber amplifiers (EDFAs) interspersed on the link. For links less than 80 km, the EDFAs were not used. However, at longer link lengths the cumulative loss from the link resulted in very-low-return optical power and insufficient SNR for a phase lock. For example, at 251 km the one-way link loss alone was 62 dB. However, with the insertion of bidirectional EDFAs, the SNR effectively decays linearly with length rather than exponentially [16], and, as found previously, the SNR is not a practical limit to long-distance frequency transport [7]. To prevent lasing and stimulated Brillouin scattering (SBS) caused by reflections from fiber connections throughout the link, the gain of any individual (isolator-free bidirectional) EDFA was limited to 7–25 dB. An optical bandpass filter ( $\sim 1$  nm FWHM) centered at 1535 nm reduced the amplified spontaneous emission that might otherwise saturate the EDFA gains.

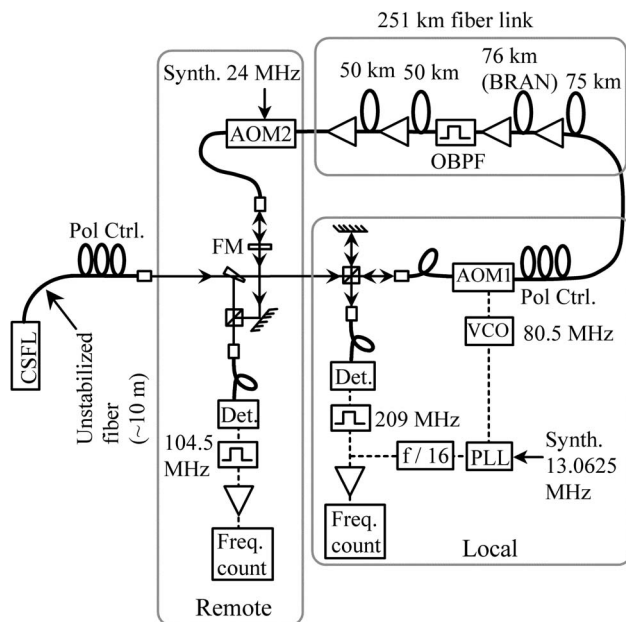


Fig. 2. Experimental setup for frequency transfer and fiber stabilization. AOM, acousto-optic modulator; CSFL, cavity-stabilized fiber laser; Det., detector; FM, Faraday mirror; OBPF, optical bandpass filter; PLL, phase-locked loop; Pol Ctrl., fiber-optic polarization controller; VCO, voltage-controlled oscillator. Thick curves are optical fiber, thin lines are free-space propagation; and dashed lines are electrical paths. Laser light is split by a wedge and cube beam splitters to act as the LO on the remote and local detectors. The remaining light is frequency shifted by AOM1 and traverses the amplified link and receives a second frequency shift from AOM2. The FM transmits 50% of the light to mix with the LO at the remote detector. The remaining light is reflected by the FM back through the link and mixes with the LO at the local detector.

### 3. PERFORMANCE LIMITATIONS

We now discuss a number of effects that limit the coherence of the transmitted signal, including measurement-related effects such as phase noise on the source, RF electronics, and receiver/transmitter interferometers, as well as link-related effects such as delay, non-linear effects, and polarization-mode dispersion. The two dominant effects are the delay-unsuppressed fiber link noise, discussed in Subsection 3.A, and the excess phase noise from the interferometer, discussed in Subsection 3.B.

In analyzing the transmitted remote signal it is most useful to consider its phase-noise power spectral density (PSD),  $S_{\text{remote}}(f)$ . The integrated timing jitter follows directly from the integral of this phase noise after dividing by  $2\pi\nu$ , where  $\nu$  is the optical frequency. The frequency instability is calculated directly from this PSD as well, using the weighting function appropriate to the desired metric (normal Allan deviation, modified Allan deviation, etc.) [17–19].

#### A. Delay Effects and Residual Fiber Noise

The length  $L$  of the fiber-optic link leads to a finite transit time  $\tau=L/c_n$  for light to propagate down the fiber, where  $c_n \sim 2 \times 10^8$  m/s is the speed of light in the fiber. As discussed in more detail in Appendix A, this delay has two effects. First, it leads to characteristic servo bumps on the phase-noise spectrum at harmonics of  $1/(4\tau)$ ; these bumps increase the overall integrated timing jitter. Second, and more important from the point of view of stability, it limits the effectiveness of one-way noise cancellation. If there is phase noise on the transmitted signal from fiber noise,  $S_{\text{fiber}}(f)$ , then even for perfect cancellation of this noise on the round-trip light, the one-way light will still suffer from delay-unsuppressed fiber phase noise of magnitude

$$S_D(f) \approx a(2\pi f\tau)^2 S_{\text{fiber}}(f), \quad (3.1)$$

as derived in Appendix A [see Eq. (A10)], where  $a=1/3$  for uniform spatial distribution of noise. This approximation holds for low Fourier frequencies  $f$ , but a complete expression valid for all  $f$  is also given in Appendix A [Eq. (A8)]. This effect is not related to any bandwidth limitation of the PLL, but is intrinsic to the fact that we are phase-locking the round-trip signal at the local end and measuring the one-way signal at the remote end. We find that in our fiber link,  $S_{\text{fiber}}(f) \propto 1/f^2$  for  $f$  below an empirical cutoff  $f_c$  (discussed in Subsection 4.B). Equation (3.1) then predicts white phase noise for  $S_D$  at frequencies below  $f_c$  and the link resonance  $1/(4\tau)$  [see Fig. 1(a)]. This delay-unsuppressed noise is a fundamental limit for this technique. Therefore, in the remainder of Section 3, we compare all other effects to Eq. (3.1).

#### B. “Local” and “Remote” Interferometer Phase Noise

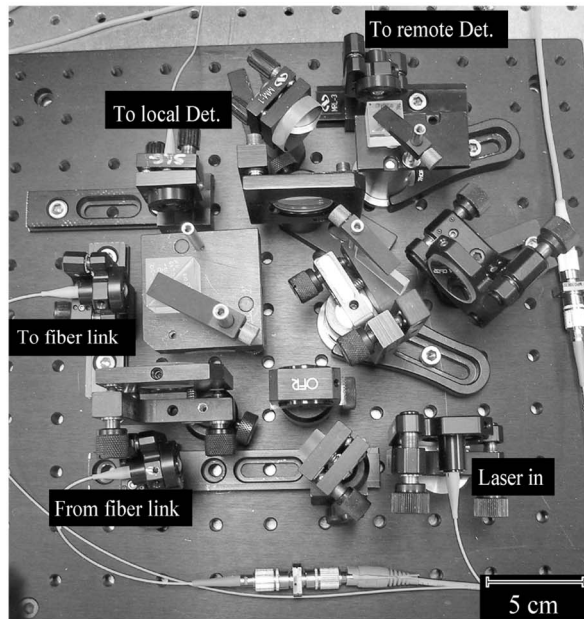
Out-of-loop paths (where LO light travels a different path from the signal light) in the local (transmitter) and remote (receiver) heterodyne interferometers are uncontrolled, and their length noise causes uncompensated

noise  $S_{\text{Int}}$  that varies as  $1/f^2$ . We desire that the interferometer's noise contribution be less than the delay-unsuppressed noise floor of Eq. (3.1), or

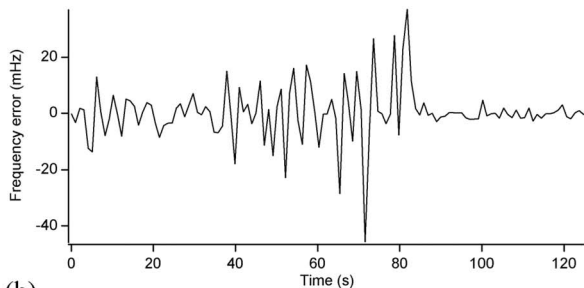
$$S_{\text{Int}}(f) < a(2\pi f\tau)^2 S_{\text{fiber}}(f). \quad (3.2)$$

Since  $S_{\text{Int}}$  diverges, we cannot satisfy condition (3.2) at arbitrarily low frequencies. Indeed, in previous experiments exploring coherent transfer over a short fiber network, out-of-loop path lengths dominated the measured instability at long gate times (low  $f$ ) [4,10]. For longer optical fiber links,  $S_{\text{fiber}}$  is correspondingly larger and the condition (3.2) can be satisfied at lower values of  $f$  (longer gate times), but ultimately  $S_{\text{Int}}(f)$  will always dominate at the lowest frequencies [Fig. 1(a)].

We minimize out-of-loop path noise by using a short path length, enclosed free-space interferometer [Fig. 3(a)]. We allow the light to propagate in optical fiber (for convenience) only when the LO and signal paths are collocated. The residual frequency instability correspond-



(a)



(b)

Fig. 3. (a) Photograph of collocated free-space transmit and receive interferometers. Dimensions  $\sim 25 \text{ cm} \times 25 \text{ cm}$ . (b) Frequency error (1 s gate time) versus time for one-way transmission of optical frequency. The interferometer is exposed to room air currents until time=83 s, when it is covered with a box for isolation, yielding a 9 dB improvement in frequency noise. For comparison, we assembled an all-fiber interferometer and found a considerably larger standard deviation of  $\sim 20 \text{ mHz}$  under the same isolated conditions.

ing to the covered free-space interferometer gives the system noise floor in Section 4 [Fig. 3(b)].

### C. Source Phase Noise

The source phase noise should be low enough to not add excess noise. For a laser with phase noise  $S_{\text{Laser}}(f)$ , the self-heterodyne contribution to the round-trip phase noise is  $S_{\text{self-het}}(f) = 4 \sin^2(2\pi f\tau) S_{\text{Laser}} \sim (4\pi f\tau)^2 S_{\text{Laser}}(f)$ . Again, we require this contribution to be less than the delay-unsuppressed residual link noise of Eq. (3.1), so that

$$S_{\text{Laser}}(f) < a S_{\text{fiber}}(f). \quad (3.3)$$

Condition (3.3) is easily met with a state-of-the-art cavity-stabilized laser. We measure an upper limit for our source of  $S_{\text{Laser}}(f) < 10^{-1} f^{-2} \text{ rad}^2/\text{Hz}$ , although the actual phase noise is likely orders of magnitude lower [20]. In Section 4, we find  $S_{\text{fiber}} \sim 10^3 f^{-2} \text{ rad}^2/\text{Hz}$  for our 251 km link, so the condition (3.3) is well satisfied. In practice our effective laser phase noise is limited by the phase noise added from the  $\sim 10 \text{ m}$  of fiber connecting the laser to the interferometer. Again, as this 10 m of fiber is substantially shorter than the link length, Eq. (3.3) is well satisfied.

### D. RF Electronic Phase Noise

It is important to minimize the cumulative phase noise of the RF electronics,  $S_{\text{RF}}$ . Since RF phase noise is additive, low RF noise requires that

$$S_{\text{RF}}(f) < a(2\pi f\tau)^2 S_{\text{fiber}}(f), \quad (3.4)$$

which is easily met for modern RF synthesizers, even for very low fiber phase noise. Furthermore, we removed any low-frequency divergence in  $S_{\text{RF}}$  by phase-locking the PLL reference synthesizer and the frequency counters to a common 10 MHz reference signal.

### E. Fiber Nonlinearities

In addition to the limit on the launched powers imposed by SBS, fiber nonlinearities can cause nonreciprocal phase noise through amplitude-to-phase noise conversion in the optical fiber [21]. However, this effect is small when a cw (as opposed to a modulated) signal is being transmitted. For a link with no EDFAs, the nonlinear phase noise is  $\delta\varphi_{\text{NL}}^2 = \gamma^2 P_0^2 \alpha^{-2} RIN_{\text{Laser}}$  or approximately  $\sim 10^{-3} RIN_{\text{Laser}}$ , where  $\gamma \sim 2/(\text{W} \cdot \text{km})$  is the fiber nonlinearity,  $P_0 \sim 1 \text{ mW}$  is the launched power,  $\alpha \sim 0.2 \text{ dB/km}$  is the fiber attenuation, and  $RIN_{\text{Laser}}$  is the laser noise. For any reasonable cw laser, the nonlinear phase noise is many orders of magnitude below the other limitations discussed here. Similarly, the phase jitter induced by the amplified spontaneous emission of the optical amplifiers in the link (similar to the Gordon-Haus effect) is also negligible compared to other limitations.

### F. Polarization-Mode Dispersion

Some researchers have reported degraded stability of their frequency transport due to nonreciprocal noise caused by PMD in the optical fiber [1,2,11,12]. However, we see no such effect in our measurements. We attribute this to the low differential group delay of our fiber link. We found  $\tau_{\text{DGD}} = 140 \text{ fs}$  for one pass of the 38 km BRAN link (see Section 4). This corresponds to a PMD coefficient

of 0.02 ps/km<sup>1/2</sup>. In contrast, PMD-induced frequency instabilities were seen in [11] where the fiber had a PMD coefficient of 0.75 ps/km<sup>1/2</sup>, which did degrade the frequency stability (before mitigation). A full treatment of the PMD effects is complicated, since it must include the polarization effects of the heterodyne detection and statistics of PMD. Here, we present a simple estimate the magnitude of the one-way phase noise due to fiber PMD and its resulting effect on the frequency instability.

For polarized light launched with its state of polarization at an angle  $\alpha$  (in the coordinates of the Poincare sphere [22]) with respect to the fast axis of a birefringent fiber, the net phase accumulated by the light propagating through the fiber is  $\varphi(t) = \Phi_{\text{iso}} + \tan^{-1}\{\cos \alpha \tan(\pi\nu\tau_{\text{DGD}})\}$ , where  $\Phi_{\text{iso}}$  is the non-polarization-dependent delay, the second term is the PMD contribution of interest, and  $\tau_{\text{DGD}}$  is the differential group delay (DGD) [23].

We see two mechanisms for fiber PMD to degrade the stability. First we estimate the phase noise from PMD due to general fiber contraction or expansion. A change in the overall fiber delay  $\delta\tau$  will produce a parasitic change in the DGD,  $\delta\tau_{\text{DGD}} = (\delta\tau/\tau)\tau_{\text{DGD}}$ . Setting  $\alpha=0$  for the maximum effect, the change in phase will be  $\delta\varphi_{\text{PMD}} = \delta\tau_{\text{DGD}}\nu\pi$ . Since fluctuations in the overall delay give exactly the one-way fiber noise,  $S_{\text{fiber}}$ , the PMD contribution to phase noise will be

$$S_{\text{fiber,PMD}} \sim (\tau_{\text{DGD}}/2\tau)^2 S_{\text{fiber}}, \quad (3.5)$$

which exceeds the delay-unsuppressed fiber phase noise [Eq. (3.1)] only at Fourier frequencies  $f < \tau_{\text{DGD}}/4\pi\tau^2\sqrt{a}$ . As an example, for our 38 km BRAN link (see Section 4),  $\tau_{\text{DGD}} = 140$  fs and  $\tau \sim 200$   $\mu$ s; the PMD effect will exceed the delay-induced effects only when  $f < 0.5$   $\mu$ Hz (a period on the order of weeks).

Environmental effects randomly change the orientation between the input polarization state and the fast axis of a birefringent fiber link, causing Doppler shifts unrelated to fiber length changes. We estimate an upper limit to this second possible PMD effect. Light switching from the fast axis to the slow axis in a time  $t_{\text{switch}}$  will give a frequency shift of  $(\delta\nu/\nu) = \tau_{\text{DGD}}/t_{\text{switch}}$ . In our link, we estimate  $t_{\text{switch}} > 36,000$  s (10 h) based on how often we must reorient the paddles for the one-way signal, yielding an upper limit of  $(\delta\nu/\nu) = 8 \times 10^{-18}$  (for the 251 km link with  $\tau_{\text{DGD}}$  estimated to be 320 fs). However, even at this low level, our measurements of frequency instability show no such PMD effects—the true  $t_{\text{switch}}$  for our setup must be even longer than our estimate.

When PMD is large enough to affect the frequency instability, a solution (for RF frequency transport) is to scramble the polarization rapidly to average out the PMD effect [1,2,12]. Such a solution would be possible for an optical frequency carrier as well, but it would be quite complicated since it would require coherent, polarization-diverse detection.

## 4. EXPERIMENTAL RESULTS

### A. Optical Fiber Link

The experiments were carried out on installed fiber from the Boulder Research and Administration Network (BRAN) in Boulder, Colo. The use of installed fiber was

critical for achieving realistic fiber link noise, and the BRAN fiber is likely particularly noisy due to its frequent excursions above ground. A short 7 km section of the link was used in [8,10]. For the longest distance experiments, the light travelled twice around Boulder on different fiber strands of the BRAN fiber, for a total length of 76 km that included  $\sim 50$  FC/PC fiber connections,  $\sim 16$  locations where the fiber exited the ground, and a total of  $\sim 1$  km of fiber passing through acoustically noisy building ductwork. In order to conduct experiments on even longer fiber links, we supplemented the BRAN fiber link with up to 175 km of spooled fiber. For the full 251 km, the round-trip link loss was about 124 dB, excluding loss from the AOMs and the interferometer. Four bidirectional EDFAs were interspersed in the link, as discussed in Section 2. The PMD of the 38 km BRAN link was measured to have a DGD of 140 fs.

### B. Measured Phase Noise and Timing Jitter on the Transmitted Signal

The measured phase-noise spectra for light traversing three different fiber links—the 38 km BRAN fiber, a 50 km spooled fiber, and the full 251 km link—are given in Fig. 5. For the same fiber lengths, the spooled fiber had 20–25 dB less noise than the installed fiber. We find that unlocked phase noise on our 251 km fiber link approximately follows a power-law dependence,  $S_{\text{fiber}}(f) \sim h/f^2$ , for  $f < f_c \sim 1$  kHz. For  $f > f_c$ ,  $S_{\text{fiber}}(f)$  drops more rapidly. For the full 251 km link, we find  $h \sim 10^3$  rad<sup>2</sup>·Hz. Since this phase noise should scale with length, we define the phase-noise coefficient  $h_L = h/L \sim 4$  rad<sup>2</sup>·Hz/km. The scaling  $S_{\text{fiber}}(f) \sim h/f^2$  is only an approximation, valid over a certain region of Fourier frequencies. In general, the environmentally induced fiber noise is expected to increase with decreasing  $f$  but will not follow a single power-law dependence on  $f$ . In that case, the expressions for the jitter or stability given below can be modified by substituting the measured  $S_{\text{fiber}}(f)$  into Eq. (3.1) and using the more general integral equations (see [17,18]) to calculate the Allan deviation.

As shown in Fig. 6 for the 251 km link, we find the measured locked phase noise to be in good agreement with that predicted by Eq. (3.1). To further explore the length dependence, Fig. 7 shows phase-noise spectra, RF power spectra, and integrated phase jitter measured at

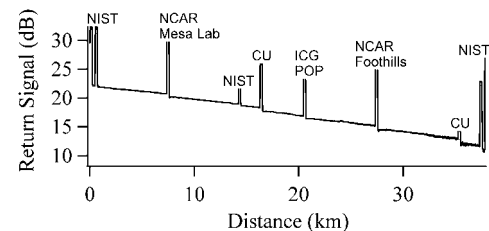


Fig. 4. Optical time-domain reflectometer (OTDR) trace for the 38 km BRAN fiber link traversing Boulder. Each spike represents a point where the fiber emerges from the ground to a patch panel. The light traveled from NIST to NCAR Mesa lab, returned on a different fiber passed by NIST again, through University of Colorado campus (CU), to NCAR foothills lab, returned on a different fiber, took the southern route around CU, and finally returned to NIST, for a total of 38 km. The same loop could be traversed again on different fiber for a total of 76 km.

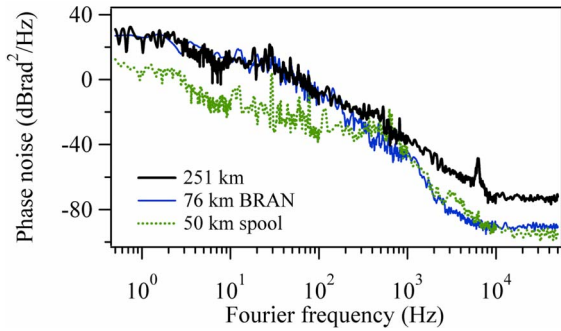


Fig. 5. (Color online) Phase-noise power spectral density for the full 251 km link (consisting of 76 km of installed fiber and 175 km of spooled fiber) for just the 76 km of installed fiber and for 50 km of spooled fiber.

different link lengths. We adjusted the link length by varying the number of spools and BRAN fiber loops in the link. Several features are evident in both the RF spectra and phase-noise spectra. Figure 7(a) illustrates that the phase noise increases quickly with length, as predicted from Eq. (3.1). In addition, strong servo bumps appear at multiples of  $1/(4\tau)$  due to the locking conditions, as discussed in Appendix A. As this phase noise increases, there is an erosion of the coherent peak in the RF spectra [Fig. 7(b)]. The length dependence of the phase noise is shown more clearly in Fig. 7(c), which plots the integrated phase noise, and corresponding timing jitter, as a function of link length. From [7] we find the simple expression for the timing jitter,  $t_{\text{jitter}} \approx v^{-1} \sqrt{ah_L f_c L \tau}$ , again assuming  $S_{\text{fiber}}(f) \sim h/f^2$  (valid for  $f < f_c \sim 1$  kHz), and excluding the servo bumps from the integral. This equation, plotted as a straight line in Fig. 7(c), predicts that the total jitter should scale approximately as  $L^{3/2}$  (since  $\tau$  scales as  $L$ ). The carrier collapse of the RF power spectra will occur when the integrated phase noise goes beyond  $\sim 1$  rad, corresponding to a timing jitter of  $\sim 0.8$  fs. In Fig. 7(c) this crossover occurs at  $\sim 80$  km link length. For quieter fiber, it would occur at a longer distance.

### C. Measured Frequency Uncertainty on the Transmitted Signal

Often the frequency instability or uncertainty is taken as the regular or total Allan deviation. For white frequency noise (i.e., phase noise that scales as  $1/f^2$ ), this choice is

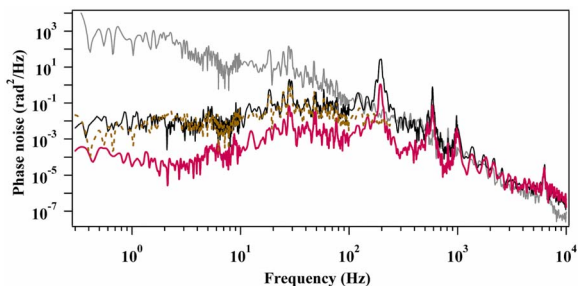


Fig. 6. (Color online) Phase-noise spectra for 251 km link of the unlocked, one-way fiber noise,  $S_{\text{fiber}}$ , (solid, gray curve); the one-way locked signal,  $S_{\text{remote}}$ , (solid, black curve); the predicted  $S_{\text{remote}}$  from Eq. (3.1) (dashed, brown curve), which is in good agreement; and the residual phase noise on the round-trip locked signal (solid, red curve).

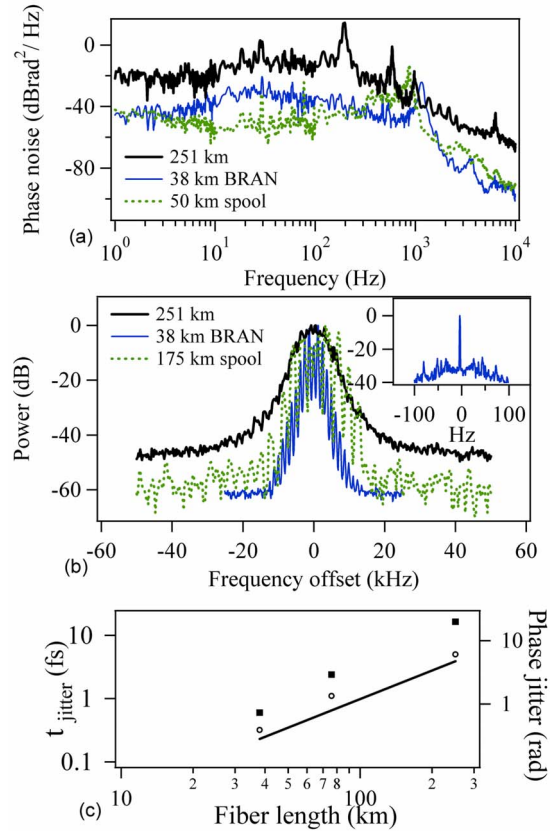


Fig. 7. (Color online) (a) Phase-noise spectra,  $S_{\text{remote}}$ , of the locked remote signal for various fiber links (the 251 and 38 km installed links yield significantly more residual phase noise due to greater intrinsic fiber noise). Note servo bumps at multiples of  $(1/4\tau)$  in frequency. (b) Locked one-way RF power spectra at 38 km with a resolution bandwidth (RBW) of 300 Hz. The servo bumps cause strong sidebands at multiples of  $1/4\tau$  (1.3 kHz) in frequency, but there remains a central coherent peak with a RBW-limited 1 Hz peak. (Inset: Expanded view of this central coherent peak with a RBW-limited 1 Hz peak). The RF power spectra at 175 and 251 km (RBW = 1 kHz) show the collapse of the coherent peak at higher phase-noise levels. (c) The timing and phase jitter versus fiber link length as in [7]; jitter integrated from 0.06 Hz to 1 MHz (solid squares); jitter excluding servo bumps (open circles). The solid line is the theoretical prediction based on integrating Eq. (3.1).

appropriate. However, for white phase noise (i.e., phase noise independent of  $f$ ), the frequency noise increases as  $f^2$ , and the regular Allan deviation diverges unless a low-frequency cutoff is invoked (and it is not always clear what the appropriate cutoff frequency might be) [17–19]. In this case, a less ambiguous metric of the frequency instability is the modified Allan deviation, which does not suffer from the same divergence issues. The use of the modified Allan deviation is more than a mathematical convenience; as shown in [18,19], it also is closely related to values returned by the frequency counter instruments used in our experiments. We therefore use it here.

The frequency instability of the transported light follows directly from the appropriately weighted and integrated phase noise. The frequency instability will be limited by the delay-unsuppressed phase noise (Subsection 3.A) for short gate times, and by the phase noise of our interferometers (Subsection 3.B) at long gate times. These two contributions are presented in Eq. (1.1) in the white

frequency noise approximation ( $f < f_c$ ),  $S_{\text{fiber}}(f) \sim h_L L / f^2$ , yielding a delay-unsuppressed phase noise of  $S_D(f) \sim a(2\pi\tau)^2 h_L L$  from Eq. (3.1). For this white phase noise, measured with gate time  $t_g$ , the corresponding modified Allan variance is [17,18]

$$\sigma_D^2(t_g, L) = \chi \frac{ah_L}{\nu^2 c_n^2} \left( \frac{L^3}{t_g^3} \right) = \kappa_D^2 L^3 / t_g^3. \quad (4.1)$$

The factor  $\chi$  has the values 3/2 for the modified Allan variance and 8 for the triangle Allan variance [17,18]. From our fiber noise  $h_L$  measured above, the optical frequency  $\nu = 195 \times 10^{12}$  Hz (1535 nm) and  $a = 1/3$ , we calculate  $\kappa_D = 8 \times 10^{-20} \text{ s}^{3/2} \cdot \text{km}^{-3/2}$  for our link for the triangle Allan variance ( $\chi = 8$ ), which is appropriate for short gate times where the counter directly averages the signal. [The actual value of  $a$  will depend somewhat on the distribution of the noise across the link as given by Eq. (A11)]. From Section 3, our approximation that the out-of-loop interferometer adds a phase noise  $S_{\text{Int}}(f)$  that varies as  $1/f^2$  leads to a corresponding modified Allan variance of  $\sigma_{\text{Int}}^2(t_g) = \kappa_{\text{Int}}^2 / t_g$  [17,18], and we empirically measure  $\kappa_{\text{Int}} = \sigma_{\text{remote}}(0 \text{ km}, 1 \text{ s}) = 2 \times 10^{-17} \sqrt{\text{s}}$ , where  $\sigma_{\text{remote}}(0 \text{ km}, 1 \text{ s})$  is the modified Allan deviation of our system with a zero link length (shorted) and measured with a gate time of 1 s. The sum of these deviations yields the total modified Allan deviation of Eq. (1.2).

To measure the fractional frequency instability, we directly counted the 104.5 MHz beat frequency generated by heterodyning the one-way (remote) light with the source light. The resulting counter data were then analyzed to give the fractional frequency uncertainty (modified Allan deviation) plotted in Fig. 8(a) for several different link lengths. Both the shapes and magnitudes follow Eq. (1.2); the uncertainty  $\sigma_{v,\text{remote}}$  falls off as  $t_g^{-3/2}$  (the delay-unsuppressed regime) until reaching the system noise floor, whereupon it falls off as  $t_g^{-1/2}$  (the interferometer noise regime). Figure 8(b) shows the measured Allan deviation at 1 s gate times, as in [7], for different link lengths, giving the expected  $L^{3/2}$  scaling. Note that the scaling of the uncertainty at short gate times follows the scaling of the integrated timing jitter, except that it does not have any added contributions from the servo bumps since they are outside of the effective low-pass filter from the counter. At long gate times, where the Allan deviation is limited by residual phase noise in the transmit and receive interferometers, the uncertainty is independent of link length.

## 5. BIDIRECTIONAL FIBER EXPERIMENTS: PERFORMANCE DEGRADATION

Fundamental to the Doppler cancellation technique is the availability of the round-trip light. However, providing this round-trip signal can be difficult in installed long-haul networks, which have EDFAs, typically equipped with optical isolators spaced every 30–100 km along the link. These optical isolators prohibit Doppler cancellation using a round-trip signal. A simple approach to overcoming this would be to send the round-trip monitor signal back to the local end through a different fiber. However, the fiber noise cancellation works only if the outbound

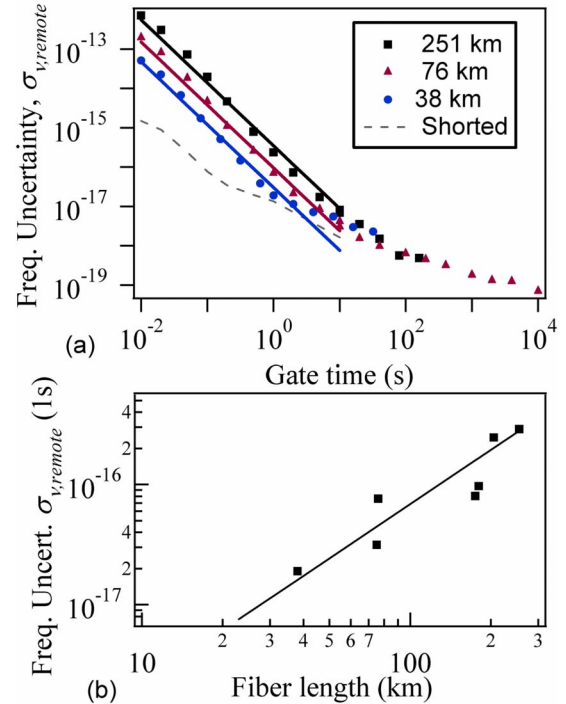


Fig. 8. (Color online) (a) Residual fractional frequency uncertainty (modified Allan deviation) versus gate time for various fiber link lengths. Shorted indicates a link length of less than 2 m. Note: as gate time  $t_g$  approaches  $\sim 100$  s, the interferometric noise  $S_{\text{Int}}$  begins to dominate. The thick solid lines illustrate the power law scaling with a  $t_g^{-1.6}$  dependence. (b) Residual fractional frequency uncertainty at a fixed 1 s gate time versus fiber link length (square points) and the prediction from Eq. (4.1). Noise differences between spooled and installed fiber contribute to the deviations from theory. All points above the curve are from links that include installed fiber; points below the curve include only spooled fiber.

phase noise exactly equals the return-trip noise, which will not be true for separate fibers. A compromise might be to use a duplexed fiber in the same cable (separated by less than 2 mm). As reported in [24], Daussy *et al.* measured the phase noise on RF frequencies propagating in two adjacent installed fibers 48 km long and found the phase noise between the two fibers to be a factor of 10 smaller than the phase noise on either individual fiber.

To explore the performance of such a stabilized duplexed link, we investigated both 400 m (spooled) and 38 km (installed) fiber links in both bidirectional and duplexed configurations. Figure 9(a) illustrates the duplexed link setup where optical circulators were used to separate the outbound and return light onto different fibers in the duplexed pair. Above 30 Hz, the one-way phase noise was controlled to a level close to the theoretical limit. At lower frequencies, there was still some suppression of the fiber noise, but the one-way phase noise began to diverge as  $1/f$ . This excess phase noise is expected to lead to a much higher frequency uncertainty. Figure 9(b) reports the delivered frequency offset (with 1 h running average) for the installed 38 km fiber link in both bidirectional and duplexed configurations. For the duplexed 38 km case, the averaged frequency error reached as much as 0.7 Hz with an approximately 24 h period. Figure 9(c) shows the resulting measured Allan deviation for both the 38 km link

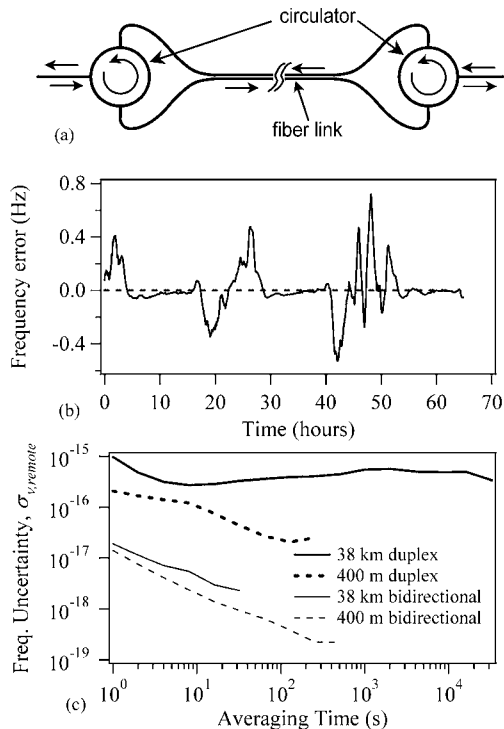


Fig. 9. (a) Experimental setup to replace bidirectional fiber link (single fiber) with a duplexed link and a pair of circulators. (b) Counted frequency error (difference from transmitted frequency) for a 1 h running average on the one-way locked signal after the 38 km link for the duplexed configuration (solid) compared to the bidirectional configuration (dashed). (c) Relative frequency instability (modified Allan deviation) for the duplexed configuration of the 38 km BRAN link and a 400 m spooled fiber compared to the instability for a bidirectional configuration for the 38 km BRAN link and a 400 m spool.

and a 400 m spool of fiber. In the duplexed configuration, both fiber lengths showed the characteristic flat dependence on gate time as a result of the flicker frequency noise. In contrast, the conventional bidirectional noise cancellation of both lengths averaged down with gate time. Since the flicker noise is not affected by the lock, we expect it to scale linearly with fiber length  $L$ .

The unidirectional nature of most existing long-haul optical fiber networks severely limits the stability of frequency transfer. Some expensive solutions could be the installation of long-haul optical fiber links dedicated to frequency transport (without isolators), or the modification of existing network structures to allow bidirectional operation of unidirectional EDFAs [25]. Perhaps older fiber networks exist that are obsolete in terms of optical telecommunications needs but would be suitable or modifiable for the more minor requirements of frequency transport. Without such approaches, long-haul frequency transport is currently not competitive with satellite-based techniques.

## 6. CONCLUSION

We demonstrate that it is possible to transfer an optical frequency over long distances in optical fiber with little degradation of the frequency stability. At short averaging times, the stability is limited by the delay-unsuppressed

fiber noise on the link, and at longer averaging times, the stability is limited by phase noise in the transmit and receive interferometers. Both of these limitations can be low, and it is possible to reach very high frequency stabilities in only tens of seconds of averaging. In contrast, the timing jitter, or phase noise, of the signal will degrade significantly with link length, scaling as  $L^{3/2}$ , due to residual noise on the fiber link. We note that these same basic limiting effects (fiber noise and out-of-loop path noise in the transceiver) will be present as well for RF-transfer techniques. However, the advantage of the optical transfer is that other noise effects are minimal. The most challenging limit is in finding (or modifying) an existing long-haul optical fiber network compatible with bidirectional frequency transfer.

## APPENDIX A

Here, we analyze in detail the phase-locked loop used in the Doppler cancellation scheme shown in Fig. 10. With the PLL inactive, the phase noise accumulated by light traveling forward in length of optical fiber starting at position  $z=0$  and exiting the fiber at  $z=L$  at time  $t$  is

$$\varphi_{\text{fiber}}(t) = \int_0^L \delta\varphi(z, t - (\tau - z/c_n)) dz, \quad (\text{A1})$$

where  $\tau = L/c_n$  is the propagation delay in the fiber,  $c_n$  is the speed of light in the fiber, and  $\delta\varphi(z, t)$  is the phase perturbation on the fiber at time  $t$  and position  $z$  with respect to some reference path. The phase noise on the round-trip light exiting the fiber at a time  $t$  is

$$\varphi_{\text{fiber,RT}}(t) = \int_0^L [\delta\varphi(z, t - z/c_n) + \delta\varphi(z, t - (2\tau - z/c_n))] dz. \quad (\text{A2})$$

The Fourier transforms of the above equations are

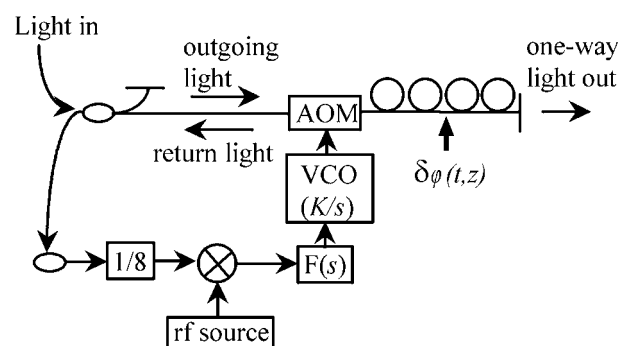


Fig. 10. Simplified schematic of the phase-locked loop for the Doppler cancellation, which defines the various contributions to the open-loop gain (A6).

$$\begin{aligned}\tilde{\varphi}_{\text{fiber}}(\omega) &= \int_0^L e^{i\omega z c_n^{-1}} e^{-i\omega\tau} \delta\tilde{\varphi}(z, \omega) dz, \\ \tilde{\varphi}_{\text{fiber,RT}}(\omega) &= 2 \int_0^L \cos(\omega(\tau - z/c_n)) e^{-i\omega\tau} \delta\tilde{\varphi}(z, \omega) dz.\end{aligned}\quad (\text{A3})$$

Assuming that the noise is uncorrelated with position, the phase-noise PSD for the fiber-induced phase noise on the one-way light is

$$S_{\text{fiber}}(\omega) = \langle |\tilde{\varphi}_{\text{fiber}}(\omega)|^2 \rangle = \int_0^L \langle |\delta\tilde{\varphi}(z, \omega)|^2 \rangle dz, \quad (\text{A4})$$

and the fiber-induced noise on the round-trip light is

$$S_{\text{fiber,RT}}(\omega) = \langle |\tilde{\varphi}_{\text{fiber,RT}}(\omega)|^2 \rangle = 2S_{\text{fiber}}(\omega)(1 + \text{sinc}(2L\omega/c_n)), \quad (\text{A5})$$

under the simplifying assumption that the noise is independent of position. The round-trip noise is four times larger than the one-way noise at low frequencies ( $\text{sinc}(0) \sim 1$ ) since it is correlated, and only two times larger at higher frequencies, where it is uncorrelated [26].

Now we consider the PLL. Using Laplace notation, the open loop gain is

$$G(s) = G_0 F(s) s^{-1} K (1 + e^{-2s\tau}), \quad (\text{A6})$$

where  $G_0$  is an overall gain including the divider and phase-to-voltage conversion of the phase detector,  $F(s)$  is the loop filter gain,  $K$  is the voltage-controlled oscillator (VCO) conversion from volts to frequency, and  $\tau$  is the one-way delay down the fiber. The usual algebra [27] yields the noise  $S_{\text{local}}$  on the phase-locked round-trip light as

$$S_{\text{local}}(\omega) = \left| \frac{1}{1 + G(\omega)} \right|^2 S_{\text{fiber,RT}}(\omega), \quad (\text{A7})$$

where we let  $s \rightarrow i\omega$  convert to frequency space (as we do freely below as well).

The open-loop gain  $G$  is constrained by stability requirements. The large delay causes phase shifts in the loop that can lead to positive feedback. This problem can be mitigated through appropriate loop filter design as in [28], but here we consider a simple proportional-integral loop filter. If we assume that the knee of the proportional-integral bode plot occurs at low frequency, then  $\arg[G(i2\pi f)] = -(\pi/2 + 2\pi f\tau)$ , passing through  $\pi$  at  $f = 1/(4\tau)$ . As the phase passes  $\pi$ , the feedback is positive, and one would expect to observe oscillations. Indeed, we do observe servo spikes at  $f = 1/(4\tau)$  and multiples thereof, but they are finite because the magnitude of the gain,  $|G(i2\pi f)| \propto \cos(2\pi f\tau)$ , vanishes at exactly these same frequencies. In operation, we typically increase the proportional gain such that the unity gain occurs at frequencies greater than  $1/(4\tau)$ . This comes at the cost of multiple servo bumps but with the benefit of increased low-frequency suppression of the noise, important for low-frequency instability. For our 251 km link, the proportional gain is set such that  $S_{\text{local}} \sim 2 \times 10^{-7} f^2 S_{\text{fiber,RT}}$

at low frequencies. The unity gain point is then  $(2 \times 10^{-7})^{-1/2} \sim 2$  kHz, and indeed we observe servo bumps at multiples of  $f = 1/(4\tau) \sim 200$  Hz, extending beyond 1 kHz.

Now consider the one-way output light. The correction signal applied to the AOM for the one-way light is  $G_0 F(s) s^{-1} K e^{-s\tau} \tilde{\varphi}_{\text{RT}}(s)$ . Again, following the usual algebra [27], the phase of the locked one-way light is

$$\tilde{\varphi}_{\text{remote}}(s) = \tilde{\varphi}_{\text{fiber}}(s) - \left( \frac{G}{1 + G} \right) \frac{\tilde{\varphi}_{\text{fiber,RT}}(s)}{2 \cosh(s\tau)}. \quad (\text{A8})$$

An exact solution for the phase-noise power spectral density on the one-way light with the PLL active can be calculated by use of (A3), (A6), and (A8) for a given loop-filter  $F(s)$  and fiber-noise  $\delta\varphi(z, t)$  profile. However, it is more instructive to consider two limits. First, well outside of the unity gain bandwidth,  $G \rightarrow 0$ , and the noise is of course the fiber noise (A4). Well within the unity gain bandwidth,  $G \rightarrow \infty$ , and Eq. (A8) together with Eq. (A3) yields

$$S_{\text{remote}}(\omega) = \left\langle \left| \int_0^L \{i - \tan(\omega\tau)\} \sin(\omega z c_n^{-1}) \delta\tilde{\varphi}(z, \omega) dz \right|^2 \right\rangle. \quad (\text{A9})$$

Since high gain is synonymous with low Fourier frequencies, we can take the limit of Eq. (A9) and assume spatially uncorrelated noise along the fiber to find the desired result,

$$S_{\text{remote}}(\omega) \approx a(\omega\tau)^2 S_{\text{fiber}}(\omega), \quad (\text{A10})$$

valid up to order  $(\omega\tau)^4$ , where we define the dimensionless moment

$$a \equiv L^{-2} S_{\text{fiber}}^{-1} \int_0^L z^2 \langle |\delta\tilde{\varphi}(z, \omega)|^2 \rangle dz, \quad (\text{A11})$$

which describes the physical distribution of the noise along the fiber and equals 1/3 for uniformly distributed noise.

## REFERENCES

1. F. Narbonneau, M. Lours, S. Bize, A. Clarion, G. Santarelli, O. Lopez, C. Daussy, A. Amy-Klein, and C. Chardonnet, "High resolution frequency standard dissemination via optical fiber metropolitan network," *Rev. Sci. Instrum.* **77**, 064701 (2006).
2. S. M. Foreman, K. W. Holman, D. D. Hudson, D. J. Jones, and J. Ye, "Remote transfer of ultrastable frequency references via fiber networks," *Rev. Sci. Instrum.* **78**, 021101 (2007).
3. A. Bauch, J. Achkar, S. Bize, D. Calonico, R. Dach, R. Hlavac, L. Lorini, T. Parker, G. Petit, D. Piester, K. Szymaniec, and P. Urich, "Comparison between frequency standards in Europe and the USA at the  $10^{-15}$  uncertainty level," *Metrologia* **43**, 109–120 (2006).
4. I. Coddington, W. C. Swann, L. Lorini, J. C. Bergquist, Y. L. Coq, C. W. Oates, Q. Quraishi, K. S. Feder, J. W. Nicholson, P. S. Westbrook, S. A. Diddams, and N. R. Newbury, "Coherent optical link over hundreds of metres and hundreds of terahertz with subfemtosecond timing jitter," *Nat. Photonics* **1**, 283–287 (2007).
5. J. C. Bergquist, W. M. Itano, and D. J. Wineland, in *International School of Physics "Enrico Fermi"*, W. Hansch and M. Inguscio, eds. (North-Holland, 1992), p. 359.

6. L. S. Ma, P. Jungner, J. Ye, and J. L. Hall, "Delivering the same optical frequency at two places: Accurate cancellation of phase noise introduced by an optical fiber or other time-varying path," *Opt. Lett.* **19**, 1777–1779 (1994).
7. N. R. Newbury, P. A. Williams, and W. C. Swann, "Coherent transfer of an optical carrier over 251 km," *Opt. Lett.* **32**, 3056–3058 (2007).
8. J. Ye, J.-L. Peng, R. J. Jones, K. W. Holman, J. L. Hall, D. J. Jones, S. A. Diddams, J. Kitching, S. Bize, J. C. Bergquist, L. W. Hollberg, L. Robertsson, and L.-S. Ma, "Delivery of high-stability optical and microwave frequency standards over an optical fiber network," *J. Opt. Soc. Am. B* **20**, 1459–1467 (2003).
9. G. Grosche, B. Lipphardt, H. Schnatz, G. Santarelli, P. Lemonde, S. Bize, M. Lours, F. Narbonneau, A. Clairon, O. Lopez, A. Amy-Klein, and C. Chardonnet, "Transmission of an optical carrier frequency over a telecommunication fiber link," in *Digest of Conference on Lasers and Electro-Optics/Quantum Electronics (CLEO)* (Optical Society of America, 2007), paper CMKK1.
10. S. M. Foreman, A. D. Ludlow, M. H. D. Miranda, J. E. Stalnaker, S. A. Diddams, and J. Ye, "Coherent optical phase transfer over a 32-km fiber with 1-s instability at  $10^{-17}$ ," *Phys. Rev. Lett.* **99**, 153601 (2007).
11. O. Lopez, A. Amy-Klein, C. Daussy, C. Chardonnet, F. Narbonneau, M. Lours, and G. Santarelli, "86-km optical link with a resolution of  $2 \times 10^{-18}$  for RF frequency transfer," (2007), <http://arxiv.org/abs/0711.0933v3>.
12. O. Lopez, C. Daussy, A. Amy-Klein, C. Chardonnet, F. Narbonneau, M. Lours, and G. Santarelli, "Fiber frequency dissemination with resolution in the  $10^{-18}$  range," in *Proceedings of IEEE International Frequency Control Symposium and Exposition (IEEE, 2006)*, pp. 80–82.
13. R. W. P. Drever, J. L. Hall, F. V. Kowalski, J. Hough, G. M. Ford, A. J. Munley, and H. Ward, "Laser phase and frequency stabilization using an optical-resonator," *Appl. Phys. B* **31**, 97–105 (1983).
14. M. Musha, Y. Sato, K. Nakagawa, K. Ueda, A. Ueda, and M. Ishiguro, "Robust and precise length stabilization of a 25-km long optical fiber using an optical interferometric method with a digital phase-frequency discriminator," *Appl. Phys. B* **82**, 555–559 (2006).
15. J. Kim, J. Chen, Z. Zhang, F. N. C. Wong, F. X. Kartner, F. Loebl, and H. Schlarb, "Long-term femtosecond timing link stabilization using a single-crystal balanced cross correlator," *Opt. Lett.* **32**, 1044–1046 (2007).
16. T. Okoshi and K. Kikuchi, *Coherent Optical Fiber Communications* (KTK Scientific Publishers, 1988).
17. D. B. Sullivan, D. W. Allan, D. A. Howe, and F. L. Walls, "Characterization of clocks and oscillators," in *NIST Technical Note 1337* (National Institute of Standards and Technology, 1990).
18. S. T. Dawkins, J. J. McFerran, and A. N. Luiten, "Considerations on the measurement of the stability of oscillators with frequency counters," *IEEE Trans. Ultrason. Ferroelectr. Freq. Control* **54**, 918–925 (2007).
19. E. Rubiola, "On the measurement of frequency and of its sample variance with high-resolution counters," *Rev. Sci. Instrum.* **76**, 054703 (2005).
20. W. C. Swann, L. Lorini, J. Bergquist, and N. R. Newbury, "Narrow linewidth  $1.5 \mu\text{m}$  sources and the thermal limit," in *Digest of IEEE LEOS Summer Topical Meetings (IEEE, 2007)*, pp. 165–166.
21. G. P. Agrawal, *Nonlinear Fiber Optics*, 3rd ed. (Academic Press, 2001).
22. E. Collett, *Polarized Light: Fundamentals and Applications* (Marcel Dekker, 1992).
23. P. A. Williams, "Modulation phase-shift measurement of PMD using only four launched polarisation states: A new algorithm," *Electron. Lett.* **35**, 1578–1579 (1999).
24. C. Daussy, O. Lopez, A. Amy-Klein, A. Goncharov, M. Guinet, C. Chardonnet, F. Narbonneau, M. Lours, D. Chambon, S. Bize, A. Clairon, G. Santarelli, M. E. Tobar, and A. N. Luiten, "Long-distance frequency dissemination with a resolution of  $10^{-17}$ ," *Phys. Rev. Lett.* **94**, 203904 (2005).
25. S.-T. Lee and C.-J. Chae, "Low-cost bidirectional optical amplifier using a unidirectional Er-doped fiber amplifier and a fiber Mach-Zehnder interferometer," *IEEE Photon. Technol. Lett.* **13**, 76–78 (2001).
26. K. H. Wanser, "Theory of thermal phase noise in michelson and Sagnac fiber interferometers," in *Proceedings of the Tenth International Conference on Optical Fiber Sensors (OFS 10)*, Proc. SPIE 2360, 584–587 (1994).
27. F. M. Gardner, *Phaselock Techniques* (Wiley, 1979).
28. B. S. Sheard, M. B. Gray, and D. E. McClelland, "High-bandwidth laser frequency stabilization to a fiber-optic delay line," *Appl. Phys. Lett.* **45**, 8491–8499 (2006).